Mechanical Systems and Signal Processing 81 (2016) 19–34

Contents lists available at ScienceDirect

Mechanical Systems and Signal Processing

journal homepage: www.elsevier.com/locate/ymssp

Periodic responses of a structure with 3:1 internal resonance

A.D. Shaw [a,*], T.L. Hill [b], S.A. Neild [b], M.I. Friswell [a]

[a] College of Engineering, Swansea University, Swansea SA2 8PP, United Kingdom
[b] Department of Mechanical Engineering, University of Bristol, Queen's Building, Bristol BS8 1TR, United Kingdom

ARTICLE INFO

Article history:
Received 24 July 2015
Received in revised form
12 March 2016
Accepted 17 March 2016
Available online 31 March 2016

Keywords:
Internal resonance
Vibration testing
Normal form
Isola

ABSTRACT

This work presents a conceptually simple experiment consisting of a cantilever beam with a nonlinear spring at the tip. The configuration allows manipulation of the relative spacing between the modal frequencies of the underlying linear structure, and this permits the deliberate introduction of internal resonance. A 3:1 resonance is studied in detail; the response around the first mode shows a classic stiffening response, with the addition of more complex dynamic behaviour and an isola region. Quasiperiodic responses are also observed but in this work the focus remains on periodic responses. Predictions using Normal Form analysis and continuation methods show good agreement with experimental observations. The experiment provides valuable insight into frequency responses of nonlinear modal structures, and the implications of nonlinearity for vibration tests.

1. Introduction

There is significant research interest in the vibrations of structures that exhibit nonlinear responses. This is due to the ubiquity of such structures; for example numerous fundamental structural forms such as plates, shells and beams will exhibit nonlinear phenomena when vibrating at sufficient amplitude. Furthermore, flexible materials exhibit nonlinear stress/strain when at large strains, and mechanisms can introduce nonlinear phenomena due to geometrical effects, as well as non-smooth nonlinearities due to friction, freeplay, impact and backlash [1–3].

In addition to the academic interest in such systems, there is strong interest within industry. This is driven by the increasing demand for lightweight and flexible structures such as large wind turbine blades, or long span bridges [1]. Furthermore, new technologies such as Micro Electromechanical Systems (MEMS) utilise structures that operate on scales where effects such as electromagnetic forces generate significant nonlinear forces [4]. Nonlinearity is also being exploited in applications such as vibration isolation [5] and energy harvesting [6].

Of particular interest is the requirement to use dynamic testing methods to characterise the vibratory response of structures in order to make performance predictions, so-called system identification. While this practice has the well established methodology of modal testing in the case of linear systems [7], the presence of nonlinearity greatly complicates this task, due to the wide range of phenomena that nonlinear systems may exhibit [8,9]. Nonlinearity introduces phenomena including amplitude dependant response frequencies, super and sub harmonic responses, and multiple stable responses to a given excitation [1]. Yet more complexity emerges when multiple degrees of freedom are present, because the principle of superposition that greatly simplifies the decomposition of linear problems no longer applies. Despite this, the concept of normal modes has been extended, initially into the so-called weakly nonlinear regime [10]. The concept of

* Corresponding author.
E-mail address: a.d.shaw@swansea.ac.uk (A.D. Shaw).

http://dx.doi.org/10.1016/j.ymssp.2016.03.008

Nomenclature

E	Young's modulus
$\vec{F}$	vector of Fourier components of the forcing signal
q_n	nth modal variable
Q_1	first modal response amplitude taken at drive frequency
Q_2	second modal response amplitude taken at third harmonic of drive frequency
$\vec{V}$	vector of Fourier components of the voltage signal sent to the shaker amplifier
u_n	resonant component of the nth modal variable
U_n	response amplitude of u_n
x	axial coordinate
z	lateral coordinate
ζ	linear modal damping ratio
θ	phase
ν	Poisson's ratio
ρ	mass density
$\phi_n(x)$	nth mode shape function
$\phi_{n,i}$, $\phi_{n,L}$	shorthand for $\phi_n(x_i)$, $\phi_n(x_L)$
ω_{nn}	linear natural angular frequency of nth mode
ω_{rn}	resonant response frequency of nth modal variable

Nonlinear Normal Modes (NNM) has since been shown to remain as an invaluable framework even when nonlinearity becomes strong [11]. Many nonlinear continuous or multi-degree of freedom systems exhibit some particularly novel responses whenever one mode of free vibration has a natural frequency that approaches an integer ratio to that of another, a condition known as internal resonance [12,11]. Forms of this behaviour have been shown in structures ranging from jointed pendulums to sagging cables [12,13].

The interest in nonlinear system identification has led to a demand for experimental demonstrators featuring continuous structures with nonlinearity; however experimental works on these types of systems are heavily outnumbered by analytical and numerical studies. In [14], Amabili presents comprehensive results on the amplitude dependence of modes of plates of different dimensions that arise due to Von Karman strains that are created by moderate amplitudes of deflection. Zaretzky and Crespo Da Silva considered one-to-one resonance between modes in different planes of a vertical cantilever subject to large amplitude and gravitational nonlinearity [15]. In a two-part paper, Rega et al. demonstrated numerous internal resonance conditions of an oscillating sagging cable [13,16]. Westra et al. use an intriguing microscopic beam with electromagnetic exciting forces to demonstrate that nonlinear effects cause one mode to affect the frequency of another [17]. Platten et al. describe a simplified experimental structure representing an aircraft wing, with two masses mounted on short beams representing pylon-mounted aircraft engines, which introduce nonlinearity via large deflections and through the joints used to attach them [18]. This structure has also been studied by Londoño et al. [19], who has also studied a nonlinear swept wing configuration [20]. Noël et al. [21] performed an experimental identification on a small space satellite structure. At the microscale, Cho et al. present an interesting study on a nonlinear coupled beam resonator, demonstrating jump phenomena and hardening softening behaviour [22].

Many further studies of this kind are based on the configuration first presented by Thouverez [23], widely known as the 'Liege beam', for example see [24,25]. This consists of a large cantilever and a far smaller cantilever, attached at the tip. The small cantilever is driven into geometrically nonlinear oscillations by the large cantilever, and may be idealised as a cubic spring attached to the tip of the large cantilever. The advantage of this approach is that the cantilever offers a straightforward underlying linear structure, which therefore greatly facilitates the recognition of nonlinear effects. Recent numerical work on this type of structure has shown that it has rich dynamics, exhibiting internal resonance effects including isolated response regions and torus bifurcations [26,27].

The current work draws on the approach of the Liege beam, but replaces the nonlinearity at the tip with a spring mechanism. This results in an experiment with straightforward underlying physics, with significant scope to adjust both the nonlinearity and the underlying linear modes of the system. The ability to adjust the underlying modes of the system means that a three-to-one internal resonance can be obtained. Stepped sine tests on this structure reveal some fascinating responses, including an experimental demonstration of an isolated region (or isola) of periodic responses, and also quasi-periodic response regions. The periodic phenomena are explained in terms of an underlying backbone structure (i.e. the free response) revealed by normal forms analysis, and show reasonable agreement with a continuation analysis of the reduced order system.

The work proceeds as follows: in Section 2 the experimental structure is described, along with discussion of how the dynamics may be tuned to internal resonance between the first two modes of the system, the linear modal properties of the beam, and the method of control. In Section 3, the decomposed equations of motion are presented, and backbone curves for the system are derived using the method of normal forms [28]. The backbone curves show that, if the first two modes are considered, three types of free resonant response are possible. In Section 4, experimental results are presented for forcing near the first modal frequency of the beam. These results fall into two groups; the first of which may be discerned with standard upward and downward stepped sine tests. The second group of results form an isola, and required a 'kick' procedure to give the initial conditions that access these results. The effect of control strategy on the accuracy of results is also described. In Section 5, the experimental results are decomposed into modal coordinates, and this is compared to results of a continuation study on the underlying modal equations. This gives the bifurcations of the forced and damped system, and

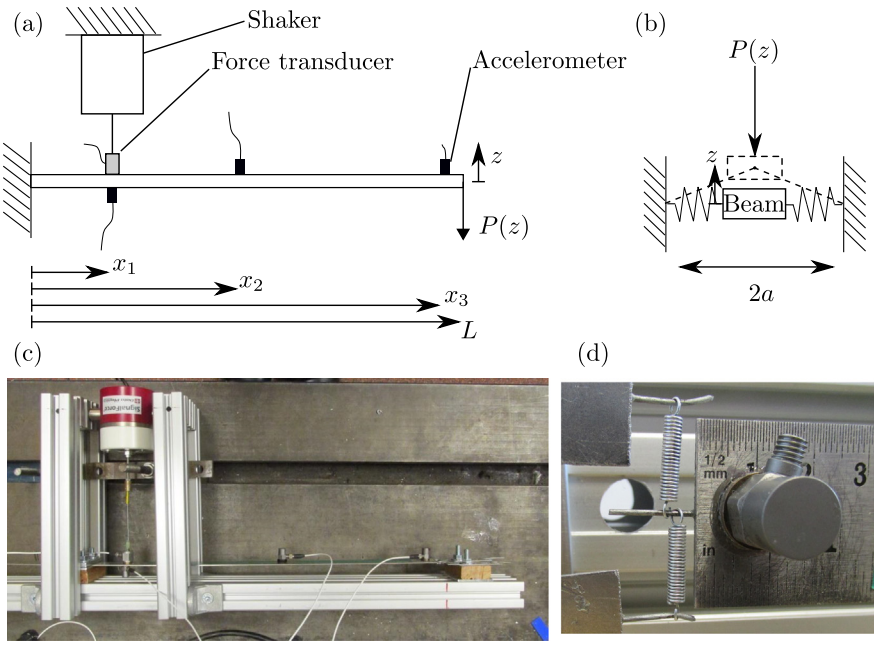

Fig. 1. (a) Schematic of the experiment. (b) Detail of nonlinear spring mechanism. (c) Photograph of experimental setup. (Some dimensions in this image differ from those used in the results.) (d) Closer perspective on the nonlinear spring mechanism.

reveals that a torus bifurcation leads to a region of quasiperiodic behaviour. An experimental example of this response is briefly presented. Finally conclusions are summarised in Section 6.

2. Experimental setup

2.1. Description of structure under test

Fig. 1(a) presents a diagram of the experiment. The main structure is a cantilever beam of length $L = 380$ mm. At its tip is a nonlinear spring mechanism, detailed in Fig. 1(b). The motion of the beam is recorded by three PCB 352 C03 piezoelectric accelerometers at axial locations $x_1 = 40$ mm, $x_2 = 150$ mm and $x_3 = 370$ mm as shown. The beam is excited by a Data Physics GW-V4 electrodynamic shaker at x_1, connected by a lightweight stinger made of 1 mm wire, and a PCB 208 C03 force transducer to record the force input to the beam.

The arrangement of springs shown in Fig. 1(b) gives rise to geometric nonlinearity at large amplitudes. The force displacement curve for this arrangement is given by:

$$P(z) = 2kz\left(1 - \frac{\ell_0}{\sqrt{a^2 + z^2}}\right) \tag{1}$$

where k is the rate of each spring, ℓ_0 is the original length of each spring and a is the half span of the mechanism. This may be approximated in the form:

$$P(z) \approx k_1 z + k_3 z^3 \tag{2}$$

by the use of a Maclaurin expansion, where $k_1 = 2k(1 - \ell_0/a)$ and $k_3 = k\ell_0/a^3$. The comparison between the exact (1) and approximate (2) forms of the nonlinearity is given in Fig. 2, showing that the mechanism is well approximated as a cubic nonlinearity.

Note that the ratio ℓ_0/a, which must be between 0 and 1 for springs to maintain tension, has an important effect on the amount of nonlinearity and the underlying linear modes of the beam. A ratio of 1 will give $k_1 = 0$, meaning that the underlying linear modeshapes of the beam will be those of a free ended cantilever, and this value will also give the maximum value for k_3 [29]. As this ratio approaches zero, the pretension in the springs will increase, maximising the linear stiffness k_1, and setting k_3 to zero. If k is sufficient the linear stiffness may restrict the motion of the beam tip, so that the linear mode shapes are similar to those of a clamped-pinned beam. Therefore the distance a, along with the length of the beam L, allows manipulation of the modes and natural frequencies of the structure. Fig. 3 shows this trend, using a classical analysis of the modes assuming that the structure is simply a cantilever with a small mass and a linear spring given by k_1 at the tip. The

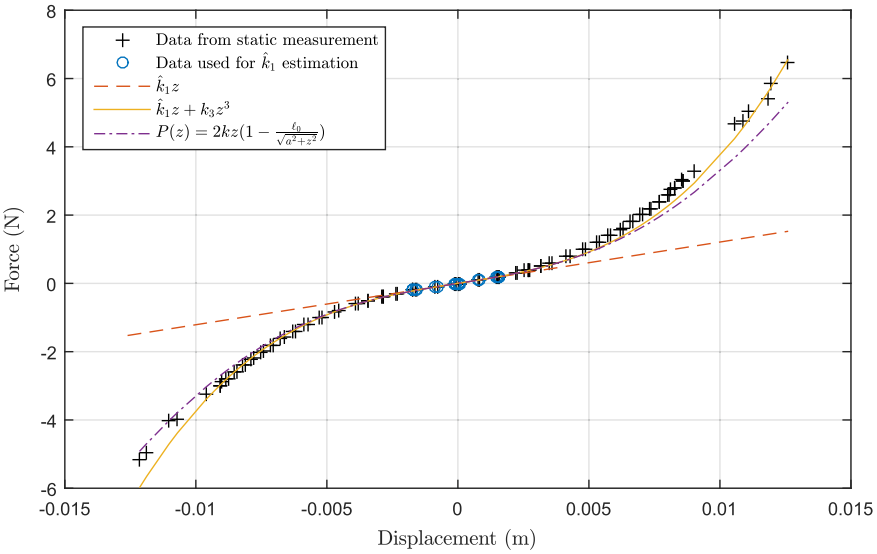

Fig. 2. Static force displacement at the tip of the beam, comparing the predicted response with the approximation and measured data.

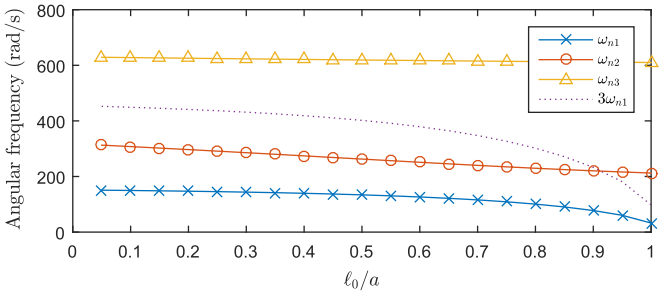

Fig. 3. Variation of modal frequencies with ℓ_0/a.

figure shows that values of ℓ_0/a of around 0.925 will give an approximate ratio of 3:1 between the 2nd modal frequency and the first; we will examine this internal resonance in detail, although clearly other internal resonances can be achieved. In the experiment that follows, the ratio $\ell_0/a = 0.957$, which gives a higher ratio of ω_{n2} to ω_{n1}; however as the response frequency of mode 1 increases due to the stiffening nonlinearity, it shall be seen that the 3:1 interaction becomes exact.

Fig. 1(c) and (d) shows photographs of the physical set up. Note that care was taken to ensure that the accelerometer cables had sufficient free length that they exerted no significant forces on the structure, but were not so long that they could form large oscillations during tests, potentially influencing test results.

2.2. Nonlinear spring measurements

The dimensions of the spring mechanism were measured to be as follows: $k = 0.910$ N mm^{-1}, $a = 18.6$ mm, $\ell_0 = 17.8$ mm. However, due to the sensitivity of Eq. (1) to these parameters, a static force–displacement measurement was performed on the beam tip in order to verify the model. This was achieved with the use of a sensitive spring-balance attached to the beam tip via a thread, with displacements measured using a laser displacement sensor (Microtrak LTC-120-40-SA). The results of this measurement are shown in Fig. 2.

As previously discussed, the linear component of the spring has a significant effect on the linearised natural frequencies and mode shapes; therefore this component was estimated using least-squares regression on the subset of data marked with circles (○) in Fig. 2, to obtain greater accuracy for this value. It was found to be $\hat{k}_1 = 0.121$ N mm^{-1}. This value includes a contribution from the beam stiffness, measured to be 0.0432 N mm^{-1} in a similar test with the springs removed. Therefore, for the spring mechanism alone, $k_1 = 0.0779$ N mm^{-1}. The cubic coefficient was estimated using a least squares regression on the data in Fig. 2 with all linear components subtracted, and found to be $k_3 = 2.516 \times 10^{-3}$ N mm^{-3}. These values compare well to the values calculated using the formulas given with (2), which predict that $k_1 = 0.0783$ N mm^{-1} and $k_3 = 2.517 \times 10^{-3}$ N mm^{-3}.

In Fig. 2 raw data is compared to the fitted linear and cubic models, and the results of Eq. (1) using the measured values

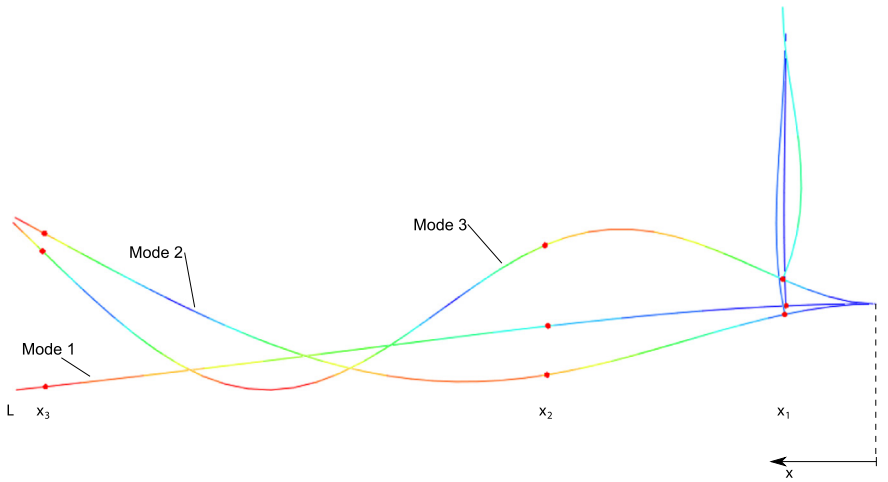

Fig. 4. FEA mode shapes of beam and stinger; red dots indicate accelerometer locations. (For interpretation of the references to colour in this figure caption, the reader is referred to the web version of this paper.)

of k, a, and ℓ_0. All of these graphs show good agreement up to displacements of approximately 7 mm in magnitude, whereupon they begin to diverge slightly. There is some asymmetry visible in the raw data.

2.3. FEA model of the underlying linear system

An FEA model created in ABAQUS was used to obtain mass normalised mode shapes for the structure. The main beam was represented by 39 beam elements (B21), with the section modelled as a rectangle with height 30 mm and breadth 1.0 mm, made from steel ($E = 210 \times 10^9$ N/m^2, $\rho = 7850$ kg/m^3, $\nu = 0.3$). It was found that the presence of the stinger caused a slight increase in the first natural frequency; this effect could not easily be eliminated on account of the high flexibility of the main structure. Therefore, the stinger was approximately modelled in the FEA model as a steel beam of circular section, 1.0 mm in diameter and 85 mm in length, using 12 elements. The node at the tip of this beam is restrained from motion in the x direction and rotation, whilst free to move in the z direction. Therefore this boundary condition approximated the sliding boundary condition imposed by the presence of the shaker. The accelerometers were represented as 10.0 g point masses; this is an approximate value as it is hard to estimate how much mass due to cabling should be included. A grounded linear spring element was located at the tip with a constant equal to k_1 as established in Section 2.2.

The resulting mode shapes are given in Fig. 4 and the frequencies and amplitudes at the sensor points and tip are given in Table 1. The FEA frequencies are compared to those measured on the experiment using low level voltage controlled sweeps, showing reasonable agreement.

2.4. Control strategy

The testing approach used is essentially a stepped sine test. However, some modification to this approach is needed for testing the nonlinear system. A nonlinear response to forced harmonic vibration typically includes higher harmonics of the main forcing frequency [30]; this contrasts with a linear system where the steady state response will be entirely at the forcing frequency. In practice, these higher harmonic responses interact with the stiffness and mass of the shaker, and thus distort the force signal that the shaker supplies to the structure. In many cases, such as when the harmonics do not affect the resonant responses of the structure, the effect is minor and may be disregarded. However, this structure features a deliberate interaction between the third harmonic of the first modal frequency and the second mode, and so this effect is potentially important.

In order to monitor and control this effect, custom signal acquisition and control software created in the Labview [31] environment was used to drive the shaker and monitor the experiment. The control strategy is based on a feed-forward method used by Barton et al. [32]. Suppose that the voltage signal sent to the shaker amplifier is approximately represented

Table 1
Linear modal properties of system where $\phi_{n,i}$ is the modeshape of the nth mode at $x = x_i$, and $\phi_{n,L}$ gives the nth modeshape at $x = L$.

Mode n	FEA ω_{nn} (rad/s)	Experiment ω_{nn} (rad/s)	$\phi_{n,1}$ (m)	$\phi_{n,2}$ (m)	$\phi_{n,3}$ (m)	$\phi_{n,L}$ (m)
1	57.30	55.92	0.125	1.35	5.13	5.34
2	193.75	199.18	−0.575	−3.86	3.80	4.67
3	552.14	551.04	1.330	3.21	2.86	4.41

as:

$$v(t) \approx \sum_i V_{c,i} \cos(i\Omega t) + V_{s,i} \sin(i\Omega t) \tag{3}$$

i.e. as a truncated Fourier series based on the drive frequency. The coefficients may be formed into a vector $\vec{V}$. A similar vector $\vec{F}$ can be created for the actual steady state force signal measured between the beam and the stinger:

$$f(t) \approx \sum_i F_{c,i} \cos(i\Omega t) + F_{s,i} \sin(i\Omega t) \tag{4}$$

The values of i used need not be consecutive, but chosen based on a compromise between speed of data acquisition and quality of input control. In this work, results are compared for three different choices:

- $i = \{1\}$ – only the drive frequency amplitude controlled.
- $i = \{1, 3\}$ – drive frequency and third harmonic amplitude controlled.
- $i = \{1, 2, 3, 4, 5\}$ – first five harmonics controlled.

It is assumed that the system comprising the electromagnetic shaker and the nonlinear structure acts as a one-to-one function i.e. $\vec{F} = \vec{F}(\vec{V})$. This assumption is locally valid, so long as no bifurcations or system changes occur. Therefore, achieving a desired force signal $\vec{F}^*$ (i.e. the required pure cosine signal) requires the numerical solution of:

$$\vec{F}(\vec{V}) - \vec{F}^* = 0 \tag{5}$$

The solution of (5) is found using a Newton–Raphson approach, using Broyden updates to reduce time required to evaluate the Jacobian matrix in a method similar that used in [32]. The maximum relative magnitude of error in solving (5) was 1%; the results given in Section 4.1.2 suggest that this tolerance permits small errors in the location of bifurcations and on harmonic responses, but has a negligible effect on the drive frequency response. Any points that failed to solve within this tolerance within a maximum number of iterations are omitted from the results, and if two consecutive points on a sweep failed the sweep was terminated. In all cases presented in this work, $\vec{F}^*$ is chosen to give a pure cosine signal; i.e. the first element is the required force amplitude and all other elements are zero.

In order to determine whether a signal had settled, the controller evaluated Fourier components up to the fifth harmonic of the force signal and the accelerometer at x_3, for each forcing period. For each signal, the components were formed into a vector, and this vector compared to that for the previous cycle. Only when the magnitude of the difference in vectors was within tolerance for both signals was the signal judged to be settled. The settling tolerance used in these results was either 0.5% or 0.25%, depending on the rate of convergence and the required accuracy traded against the execution speed of the sweep.

3. Backbone curve analysis

In order to understand the underlying behaviour of the beam structure, we consider its backbone curves. Backbone curves describe the response of the unforced, undamped equivalent system, and can be used to gain an understanding of how the structure will respond when subjected to forcing and damping [33,34]. To find the backbone curves we use the second-order normal form technique [28]. The analytical nature of this technique, along with its ability to describe harmonics, allows for additional insight into the nature of the responses.

Assuming that the forcing is sinusoidal, the forced and damped modal equation of motion is written

$$\ddot{\mathbf{q}} + \mathbf{\Lambda}\mathbf{q} + \mathbf{N}_q(\mathbf{q}, \dot{\mathbf{q}}) = \mathbf{P}_q \cos(\Omega t) \tag{6}$$

where Ω denotes the forcing frequency and where it is assumed that the response is dominated by the first two modes, such that:

$$\mathbf{q} = \begin{pmatrix} q_1 \\ q_2 \end{pmatrix}, \quad \mathbf{\Lambda} = \begin{bmatrix} \omega_{n1}^2 & 0 \\ 0 & \omega_{n2}^2 \end{bmatrix}, \quad \mathbf{P}_q = F\begin{pmatrix} \phi_{1,1} \\ \phi_{2,1} \end{pmatrix},$$
$$\mathbf{N}_q = \begin{pmatrix} 2\zeta\omega_{n1}\dot{q}_1 + \phi_{1,L}k_3(\phi_{1,L}q_1 + \phi_{2,L}q_2)^3 \\ 2\zeta\omega_{n2}\dot{q}_2 + \phi_{2,L}k_3(\phi_{1,L}q_1 + \phi_{2,L}q_2)^3 \end{pmatrix}. \tag{7}$$

From this we find the backbone curves by first setting the forcing and damping to zero, i.e. $\zeta = 0$ and $F = 0$. This allows us to write $\mathbf{N}_q$ as

$$\mathbf{N}_q = \begin{pmatrix} \phi_{1,L} \\ \phi_{2,L} \end{pmatrix} k_3[\phi_{1,L}^3 q_1^3 + 3\phi_{1,L}^2\phi_{2,L} q_1^2 q_2 + 3\phi_{1,L}\phi_{2,L}^2 q_1 q_2^2 + \phi_{2,L}^3 q_2^3] \tag{8}$$

where the cubic approximation to the nonlinearity, Eq. (2), has been assumed. Next, we separate the modal responses into resonant and non-resonant components, written $\mathbf{u}$ and $\mathbf{h}$ respectively, such that $\mathbf{q} = \mathbf{u} + \mathbf{h}$. Assuming that the resonant responses are sinusoidal, we may write

$$u_n = U_n \cos(\omega_{rn} t - \theta_n), \tag{9}$$

where u_n is the resonant component of the nth mode and where U_n, ω_{rn} and θ_n are the amplitude, frequency and phase of u_n respectively. Note that ω_{rn} and ω_{nn} are distinct, and represent the resonant response frequency and linear natural frequency respectively. Here, it is known that the resonant component of the second linear mode responds at three times that of the first linear mode, hence we choose $\omega_{r1} = \Omega$ and $\omega_{r2} = 3\Omega$.

We now apply the second-order normal form technique, as described in [28,33–35], which results in the frequency–amplitude relationship

$$\{(\omega_{n1}^2 - \Omega^2) + \frac{1}{4}[3\alpha_0 U_1^2 + 3p\alpha_1 U_1 U_2 + 6\alpha_2 U_2^2]\} U_1 = 0, \tag{10a}$$

$$(\omega_{n2}^2 - 9\Omega^2) U_2 + \frac{1}{4}[p\alpha_1 U_1^3 + 6\alpha_2 U_1^2 U_2 + 3\alpha_4 U_2^3] = 0, \tag{10b}$$

where $\alpha_i = k_3 \phi_{1,L}^{4-i} \phi_{2,L}^i$. It is found that, on the backbone curves, the resonant responses, u_1 and u_2, may either be in-phase, such that $3\theta_1 - \theta_2 = 0$, or in anti-phase, such that $3\theta_1 - \theta_2 = \pi$. These two cases result in different values of p, such that

$$p = \begin{cases} +1 & \text{when} \quad 3\theta_1 - \theta_2 = 0, \\ -1 & \text{when} \quad 3\theta_1 - \theta_2 = \pi. \end{cases} \tag{11}$$

Aside from the trivial solution to Eqs. (10), where $U_1 = U_2 = 0$, there exists a single-mode backbone curve in which $U_1 = 0$, denoted S_2. This is given by

$$S_2: \quad U_1 = 0, \quad 4(\omega_{n2}^2 - 9\Omega^2) + 3\alpha_4 U_2^2 = 0. \tag{12}$$

Another set of solutions exist when $U_1 \neq U_2$ and $U_2 \neq 0$. In this case, from Eq. (11), two sets of solutions (or backbone curves) exist – one in-phase solution where $p = +1$, and one anti-phase solution where $p = -1$. These two cases are denoted $S_{1,2}^+$ and $S_{1,2}^-$ respectively (or $S_{1,2}^\pm$ when referring to both). From Eqs. (10) these backbone curves have frequency-amplitude relationships described by

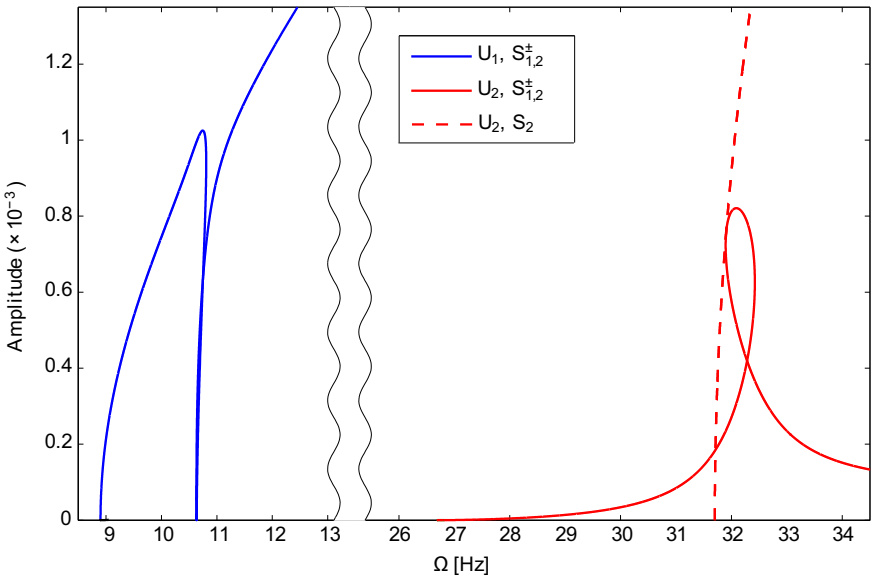

Fig. 5. Backbone curves representing the undamped and unforced responses of the structure.

$$S^{+}_{1,2}: \quad \begin{aligned} \Omega^2 &= \omega_{n1}^2 + \frac{3}{4}[\alpha_0 U_1^2 + \alpha_1 U_1 U_2 + 2\alpha_2 U_2^2], \\ \Omega^2 &= \frac{\omega_{n2}^2}{9} + \frac{1}{36}[3\alpha_4 U_2^2 + 6\alpha_2 U_1^2 + \alpha_1 U_1^3/U_2], \end{aligned} \tag{13a}$$

$$S^{-}_{1,2}: \quad \begin{aligned} \Omega^2 &= \omega_{n1}^2 + \frac{3}{4}[\alpha_0 U_1^2 - \alpha_1 U_1 U_2 + 2\alpha_2 U_2^2], \\ \Omega^2 &= \frac{\omega_{n2}^2}{9} + \frac{1}{36}[3\alpha_4 U_2^2 + 6\alpha_2 U_1^2 - \alpha_1 U_1^3/U_2]. \end{aligned} \tag{13b}$$

These backbone curves are represented in Fig. 5, where the U_2 components have been shown to be responding at 3Ω, demonstrating that the resonant component of q_2 is responding at 3 times that of q_1. It is important to note, however, that the U_1 and U_2 solutions in $S^{\pm}_{1,2}$ occur simultaneously.

Proceeding from low frequency, the U_1 and U_2 components of the $S^{\pm}_{1,2}$ solution begin at ω_{n1} and $3\omega_{n1}$ respectively, and then proceed along the $S^{-}_{1,2}$ backbone curve. Initially it forms a classically stiffening response, but as the response frequency of u_2 approaches the second linear natural frequency, ω_{n2}, U_1 rapidly approaches zero as U_2 increases. The point at which $U_1 = 0$, corresponds to the point at which the $S^{\pm}_{1,2}$ and S_2 backbone curves share a solution. It is also at this point that the $S^{\pm}_{1,2}$ solution switches from $S^{-}_{1,2}$ to $S^{+}_{1,2}$. This demonstrates the transition from an anti-phase response between u_1 and u_2, to an in-phase response. Additionally, the S_2 branch produces a response identical to that of a single degree of freedom Duffing oscillator. Whilst this is an interesting feature of the response, the remainder of this document focusses on the two-mode responses relating to the $S^{\pm}_{1,2}$ branch.

In order to gain insight into how the behaviour of these modes manifests in the response of the physical structure, we may use the second-order normal form technique to describe the response at the tip of the beam. This also allows us to compare the magnitude of the predicted tip displacements to Fig. 2, to ensure that the cubic approximation is valid. To find the tip displacements, however, we must also consider the non-resonant components of these modes. The method for finding the non-resonant components is detailed in [28,35] and results in modal displacements written $q_1 = u_1 + \sum_{i=\{3,5,7,9\}} h_{1,i}$ and $q_2 = u_2 + \sum_{i=\{1,5,7,9\}} h_{2,i}$, where $h_{n,i}$ is the component of the nth mode responding at $i\Omega$. From this, we may then find the tip displacement, z, using $z = \phi_{1,L} q_1 + \phi_{2,L} q_2$, and hence find the maximum tip displacement. This is shown in Fig. 6, from which it can be seen that for $\Omega \leq 12$ Hz the displacement remains within levels where the cubic approximation to the force displacement is almost exact, as shown in Fig. 2. Beyond this frequency, the cubic approximation begins to lose accuracy. Fig. 6 shows a very complex shape in the region of $\Omega \approx \omega_{n2}/3$, caused by the interaction and complicated response of the two modes; however this response is not seen in the forced and damped experiment, where fold and torus bifurcations will be shown to prevent periodic measurements in this region.

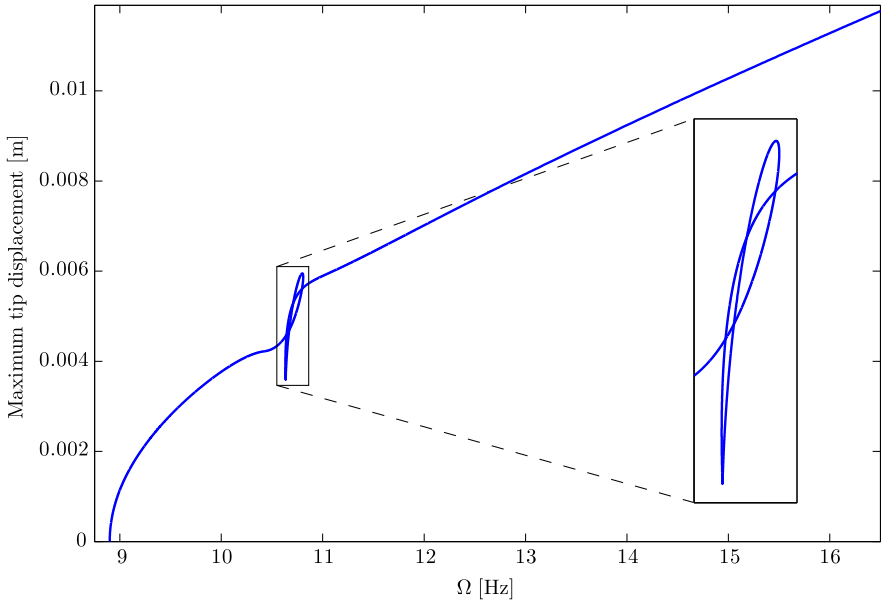

Fig. 6. Peak tip displacement of free response.

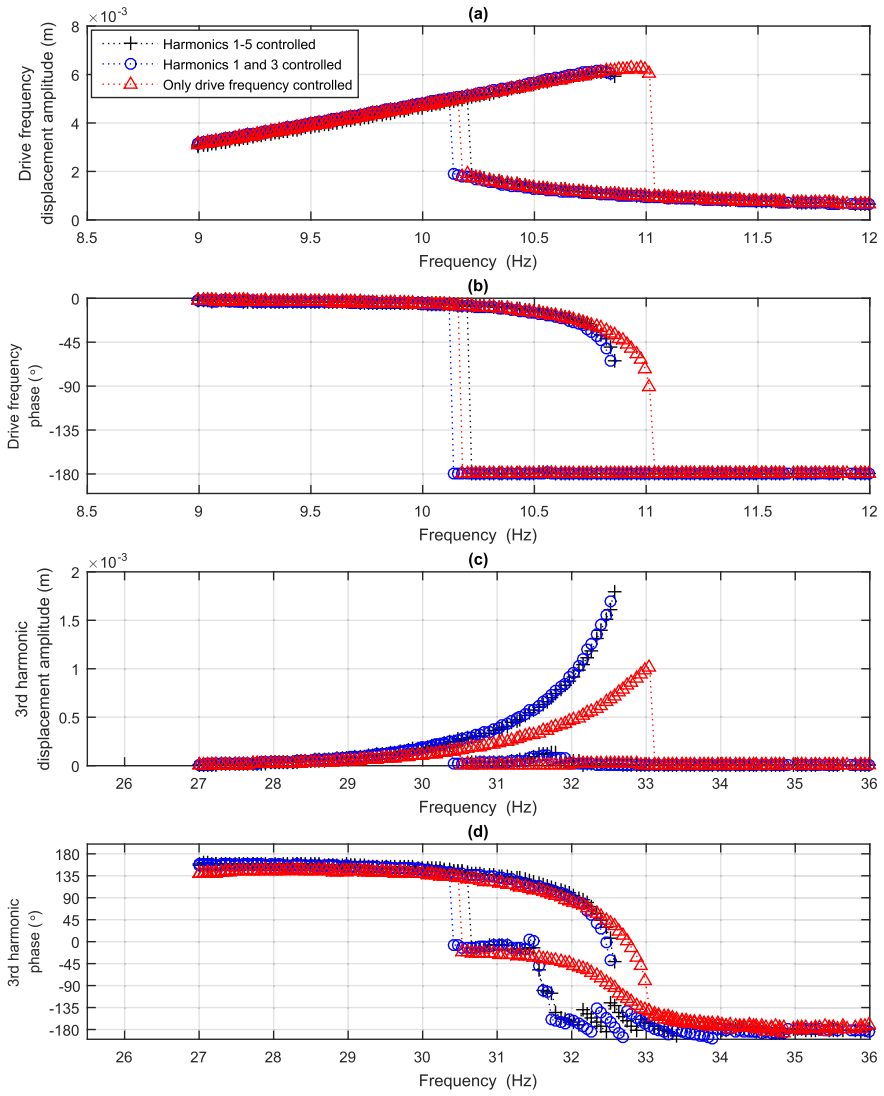

Fig. 7. Displacement amplitude response to stepped sine tests at forcing amplitude 2.0 N, taken at x_3, comparing the effect of control strategy on the main resonant branch. (a) Drive frequency amplitude. (b) Drive frequency phase. (c) 3rd harmonic amplitude. (d) 3rd harmonic phase.

4. Results

We now consider the experimental forced and damped response, and the effect that the complex backbone structure shown in the previous section has on the observed phenomena. The results of the dynamic tests are split into three sub-sections. Firstly, Section 4.1 presents results found with simple upward and downward stepped-sine sweeps, and it is seen that these can only uncover responses around the $S^{-}_{1,2}$ backbone. Then Section 4.2 discusses results from the $S^{+}_{1,2}$ backbone region, which are isolated from the $S^{-}_{1,2}$ results and therefore need an additional method to create the appropriate initial conditions. Finally, Section 4.3 briefly highlights a quasiperiodic region that lies between these two sets of responses.

4.1. Standard stepped sine sweeps

4.1.1. Response with control on first five harmonics

Fig. 7 shows the effect that the three controller options (described in Section 2.4) have on standard stepped-sine tests. All plots show results of stepped-sine sweeps, in both upwards and downwards frequency directions, with a forcing amplitude of 2.0 N. This section will give an overall description of the response in Fig. 7 where the first five harmonics are controlled. The effect of varying this control strategy will then be examined in Section 4.1.2.

The upwards sweep follows the path of the upper branch as shown in Fig. 7(a), however it was found that the response did not encounter the classic 'jump down' as seen on many SDOF systems [1]. Instead, the solving algorithm simply failed to

provide a forcing signal within tolerance or with adequate settling, and hence the sweep was terminated after two consecutive data points failed to resolve the correct signal. The failure of the control to find a settled periodic response branch suggests that a quasiperiodic response region was encountered; further investigation on this is presented in Section 4.3. Note that the limits of this upper branch are slightly greater than one third of the second modal frequency as given in Table 1; a strong interaction with the second mode is occurring. The downward frequency sweep performs the classic 'jump up' seen on SDOF systems, and at lower frequencies produces very similar results to the upward sweep. As the system 'jumps', the assumptions on which the solver proceeds are clearly violated, however typically it succeeds in calculating a new Jacobian and then converges to the new response branch.

Fig. 7(b) shows that on the upward sweep, the drive frequency phase seems to indicate that the end of the upper branch is near as it falls from 0° towards -90°. However, on the downward sweep there is little indication from this graph, or any other, that a 'jump up' is nearby.

Fig. 7(c) shows that the third harmonic amplitude reaches a significant proportion of the drive frequency amplitude when on the upper branch. There is also a small peak near 31.7 Hz on the downward sweep. This may be explained by the fact that the control algorithm permits very small 3rd harmonic components in the force signal; provided that they are of a magnitude less than 1% of $\| \vec{F} \|$ they will not cause the signal to be deemed out of tolerance. These components excite the 3rd mode only, causing the small peak to occur around the S_2 branch. The magnitudes of all other harmonics did not exceed orders of magnitude of 10^{-5} m and hence they are not shown.

The phase of the 3rd harmonic θ_3 is shown in Fig. 7(d) and shows a clear trend on the upper branch. (For the kth harmonic, response is defined as $A_k \cos(k\Omega t + \theta_k)$ where θ_k is the phase.) Starting at 160° it falls with increasing frequency in a similar manner to the phase of the drive frequency component, initially at a slow rate and then more rapidly as the limit of the branch is reached, at which point the phase is -45°. On the lower branch, the 3rd harmonic phase is somewhat noisy, due to the presence of very small harmonic components within the forcing signal. However, it may be seen that either side of 31.7 Hz (the 2nd linear modal frequency) the phase completes a familiar 180° transition.

4.1.2. Effect of alternative control options

Fig. 8 shows a typical time trace of the force signals with different control options, highlighting the distortion of the force signal, caused by the harmonic interactions with the shaker.

The difference in the response obtained by controlling the first 5 harmonics and simply controlling the drive frequency amplitude and third harmonic is shown to be negligible in Fig. 7. This corroborates the insight that only the 3rd harmonic becomes resonant, and therefore only this harmonic has a significant effect on the response. It is advantageous to reduce the fewest harmonic terms possible with this control method, because this reduces the time taken to calculate Jacobians and solve the signal, and therefore significantly reduces the overall sweep time. Therefore, insights regarding which harmonic terms can become resonant should be used in this form of testing to allow data to be gathered more rapidly.

However, substantial differences in the frequency response given in Fig. 7 are visible when only the drive frequency component is controlled. Firstly, there is a difference of approximately 0.2 Hz in the location of the peak amplitude on the upper branch; hence the control or lack thereof on the 3rd harmonic has a significant effect on the drive frequency response. This is accompanied by a change in the drive frequency phase in the peak region. Secondly, there is a large difference in the magnitude of the 3rd harmonic. Finally, it can be seen in Fig. 7(d) that this method gives a much smoother phase response for the third harmonic, because it generates no voltages at frequencies other than the drive frequency and therefore noise is not present in the low amplitude response.

The comparison between the different control strategies shows that for this type of structure, it is important to control the signal harmonics. However, this can lead to sweeps taking an excessive amount of time, so the degree of control must be a compromise between available test time and the quality of results. Caution must be exercised if choosing to only control the drive frequency amplitude, as it is generally not possible to model the effect that shaker interactions have on the results. An optimal compromise would seem to be to control all harmonics that may become resonant, as this yields in this case almost identical results to controlling all of the first five harmonics.

4.1.3. Effect of forcing amplitude variation

Fig. 9 shows stepped-sine test results repeated over a range of different forcing amplitudes. Drive frequency and third harmonic control is used, as it provides a suitable compromise between sweep time and accuracy.

Considering the upper branch in Fig. 9(a), it is apparent that the response is relatively insensitive to the forcing amplitude. For example, the drive frequency response amplitude at 9.0 Hz increases by just 33% in response to increasing the force amplitude from 1.6 N to 4.0 N, an increase of 150%. Furthermore, the frequency at the peak amplitude of the upward sweep is also somewhat insensitive to these changes in forcing amplitude, varying by approximately 1% over the range of forcing considered. This is in contrast to typical frequency responses for nonlinear SDOF systems, where increases in forcing give steady increases in both peak frequency and peak amplitude [1]. The fact that forcing amplitude makes such little difference to the peak frequency suggests that the underlying backbone structure is having a dominant effect on response.

In general, the downward sweep shows a more proportional relationship between force amplitude and response amplitude, and initially the jump up frequency increases steadily with increases in forcing amplitude. However, as the jump up frequency becomes almost equal to the peak frequency, the jump up frequency again appears to converge towards a maximum; indeed the jump frequency at 4.0 N forcing is slightly less than that for 3.6 N.

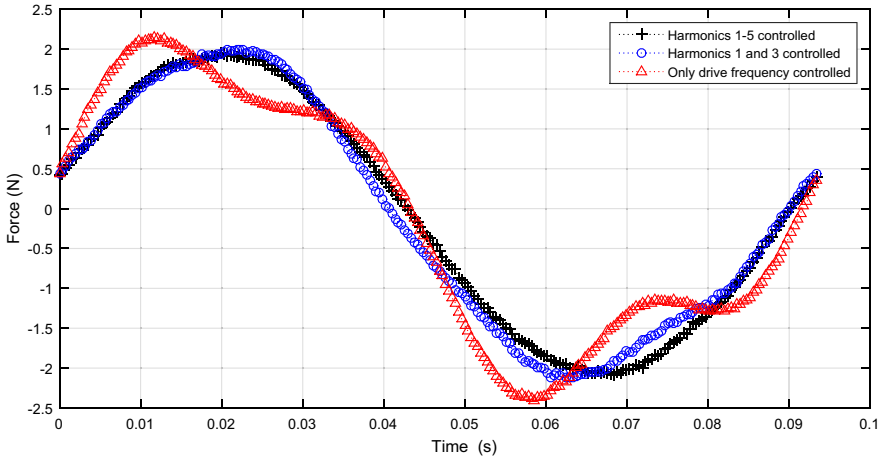

Fig. 8. Forcing signal time traces for upper branch at 10.68 Hz.

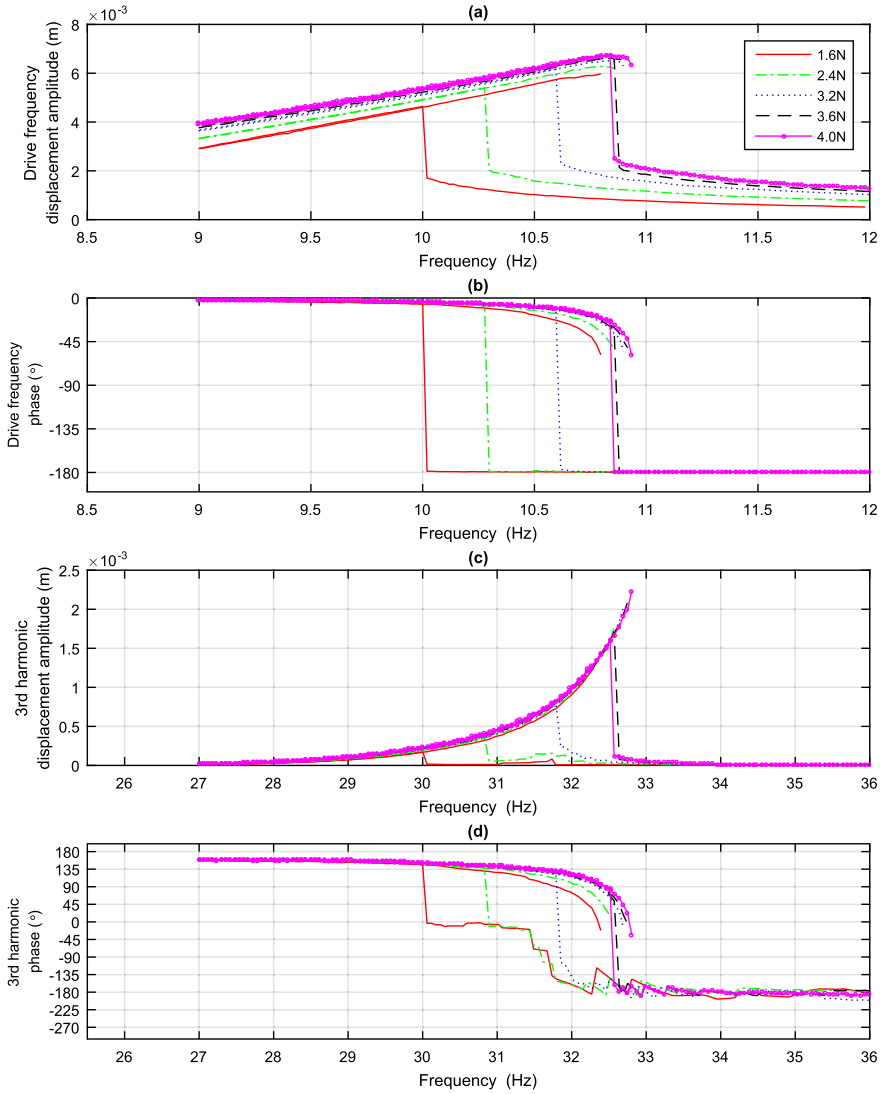

Fig. 9. Displacement amplitude response to stepped sine tests, taken at x_1, comparing the effect of varying forcing amplitude. (a) Drive frequency amplitude. (b) Drive frequency phase. (c) 3rd harmonic amplitude. (d) 3rd harmonic phase.

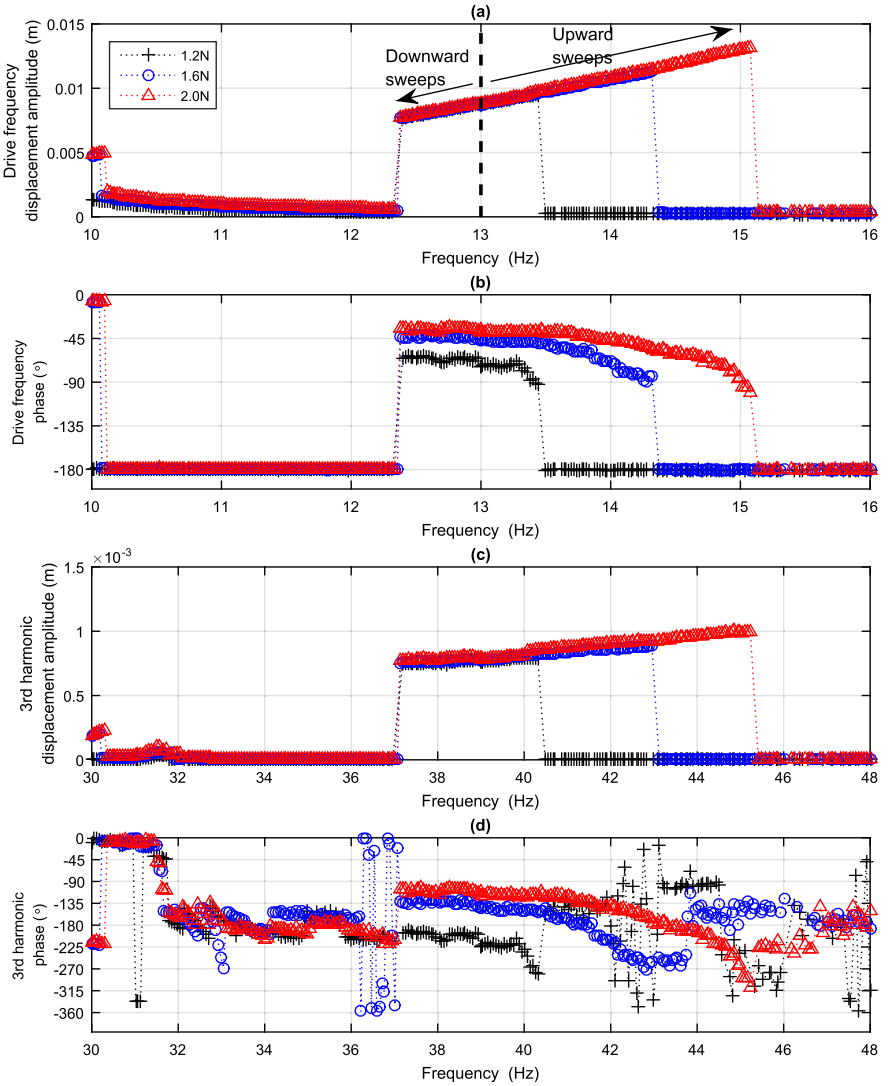

Fig. 10. Displacement amplitude response to stepped sine tests, taken at x_1, comparing the effect of varying forcing amplitude in the isola region. (a) Drive frequency amplitude, where vertical dashed line indicates start frequency for all scans following kick procedure. (b) Drive frequency phase. (c) 3rd harmonic amplitude. (d) 3rd harmonic phase.

Fig. 9(b) shows the phase of the drive frequency responses. As the phase falls with increasing frequency on the upper branch, it never passes $-60°$ before the branch is lost. As before, on the lower branch, the phase offers no clue as to the whereabouts of nearby jump up frequencies.

Parts (c) and (d) of Fig. 9 show the response of the 3rd harmonic, with similar results to those seen in Fig. 7, with phase falling from 160° down to $-45°$.

4.2. Results from the isola region

4.2.1. Method for accessing the isola response

Analysis of similar structures indicates that stable periodic responses on the $S^{+}_{1,2}$ branch form an isola region [26,27]. Therefore a process for 'kicking' the structure into this response region was established as follows:

1. Using a simple voltage controlled signal, sweep up from low frequency to 10.8 Hz, ensuring that response remains on the upper branch in the main resonant branch.
2. Simultaneously increase the voltage to a level well in excess of that typically required during tests, and increase the frequency to 13.0 Hz.
3. Allow the solver to adjust the force to the desired level (with control of harmonics as required).
4. Begin stepping in either frequency direction, recording data as before.

4.2.2. Isola results with varying forcing amplitudes

Fig. 10 shows 6 different sweeps superimposed; each sweep begins at 13.0 Hz following the 'kick' procedure described in Section 4.2.1. Then three different forcing amplitudes are used to sweep in both upwards and downwards frequency directions. In all results, the drive frequency and third harmonics were controlled as a compromise between speed of data gathering and accuracy. In trial runs, this method showed small differences to the results at the highest amplitudes (above 15 Hz forcing frequency or 13 mm forcing amplitude), when compared to sweeps where all five harmonics were controlled. This was the only time where controlling the first five harmonics gave a noticeably different response to just controlling the third harmonic, and can be attributed to the fact that the amplitude in this region is outside the range where the cubic fit is an accurate approximation to the true response as shown in Fig. 2.

As can be seen in Fig. 10(a), the isola features two jump down frequencies, referred to here as the upper and lower drop down frequencies. The lower drop down frequency is encountered by sweeping downward in frequency from the starting frequency, and the upper jump down is encountered by sweeping upward.

Fig. 10(b) shows that the upper jump down occurs as the phase reaches approximately 90°, in a manner familiar to nonlinear SDOF oscillators. There is no apparent indication from the drive frequency phase regarding the lower jump down frequency.

The figure shows that the forcing amplitude has almost no effect on the response amplitude in the isola region, but it has a significant effect on the phase and the upper jump down frequency. The variation in upper jump down frequency suggests that this is determined by the balance between energy addition due to forcing and energy dissipation due to damping [34].

In contrast to this, the lower jump down frequency shows hardly any variation due to forcing amplitude. This suggests that it is being determined by features in the underlying backbone structure, not by the energy balance between forcing and damping.

4.3. Torus response

In Section 4.1.1 it was noted that the upward sweep appeared to be terminated by a quasiperiodic or torus response instead of a typical drop down. The control strategy used for the experiment cannot be used to investigate quasiperiodic responses in detail, because it relies on the response and the force signal being periodic with the chosen forcing frequency. However, in order to verify that this region did indeed show quasiperiodic response, the kicking procedure of Section 4.2.1 was followed, and then a harmonic signal at a frequency of 11.5 Hz was applied with no control. An excerpt of the resulting time series data is shown in Fig. 11 showing that the time series is no longer periodic in the forcing period; the response was observed for sufficient time to ensure that it was not a transient beating effect. While a thorough investigation of this type of response is beyond the scope of this work, Fig. 11 is sufficient to confirm that a region of quasiperiodic resonant response exists between the regions of periodic response.

5. Comparison of results to theory

In order to compare experimental results with predictions from theory, data from all three accelerometers are used to extract a frequency response in terms of modal variables using the FEA mode shapes presented in Table 1. Fig. 12 shows the results of this, with the modal amplitudes compared to backbone curves from Eq. (13) for both $S^{-}_{1,2}$ and $S^{+}_{1,2}$ branches, plotted

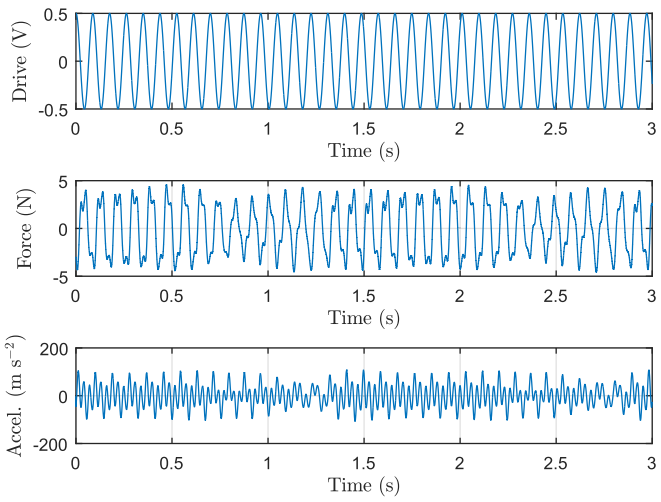

Fig. 11. Time series of a voltage controlled forced torus response, showing drive voltage signal, force signal and tip accelerometer signal.

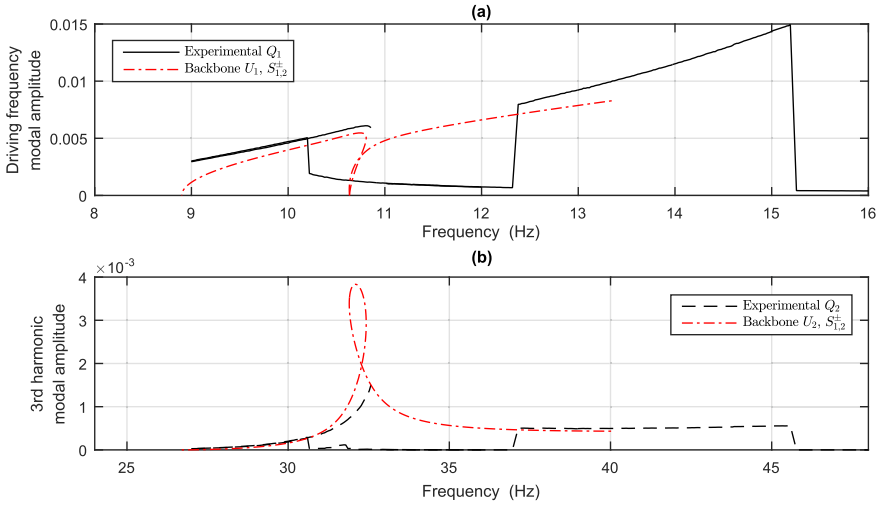

Fig. 12. Comparison of experimental results to cubic backbones using Eq. (13), with modeshapes scaled to give unit tip displacement. Forcing amplitude is 2.0 N. Part (a) shows the first modal amplitude at the drive frequency Q_1 compared to the first modal backbone U_1. Part (b) shows the second modal amplitude at the third harmonic Q_2 compared to the second modal backbone U_2.

over the approximate cubic range of the nonlinear spring. As expected, the experimental forced and damped response is seen to be strongly influenced by the predicted response of the underlying conservative system. In Fig. 12(a), the initial peak due to the first modal response at 10.8 Hz is seen to coincide with the loop region of the backbone curves, and in part (b), the second modal amplitude is also seen to remain close to its associated backbone.

To obtain the numerical forced and damped steady state solutions to Eq. (6), a continuation analysis was performed using the software AUTO [36], with the results compared to modal responses in Fig. 13. The modelling used the exact form of Eq. (1) to couple the first two modes, so that errors due to cubic approximation were not present at higher amplitudes. The modal frequencies chosen were those observed in experiment, as the response was extremely sensitive to these values.

Linear modal damping was assumed, with the damping ratio ζ equal to 1% for both modes, chosen to give a good fit to the data. It was found that the continuation results were highly sensitive to the chosen damping ratio, and that different values of damping ratio could improve the fit in some regions of the response, to the detriment of the fit in other regions. It is likely that a more sophisticated damping model, allowing different damping ratios for each mode, non-proportional damping or even nonlinear damping would deliver improved accuracy; however a rigorous means of fitting such a model is beyond the scope of this work. Overall, the chosen value gives a good general match to the experimental data, especially considering that the true damping is highly unlikely to follow such a simple model.

The features of Fig. 13 where there is a poor match between experiment and continuation are the upper and lower drop down frequencies of the isola region. One possible cause of this mismatch is the choice of damping model. In the case of the

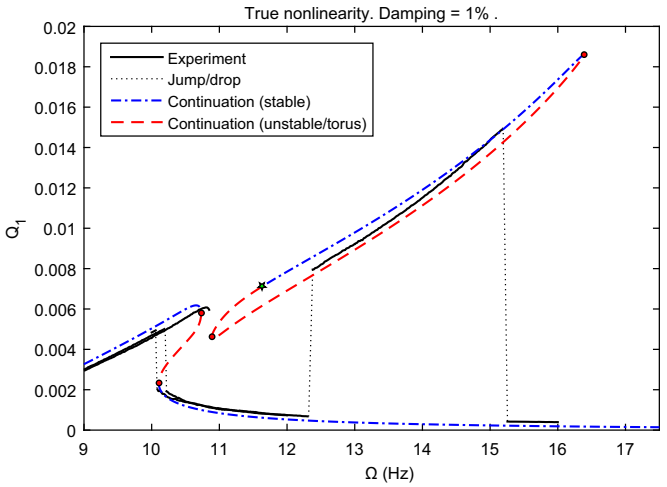

Fig. 13. Comparison of experimental results to continuation model using Eq. (1). Q_1 represents the amplitude of the first modal variable at the drive frequency, with the modeshape scaled to give unit tip displacement. Forcing amplitude is 2.0 N. Circular markers on continuation results indicate fold bifurcations, star indicates a torus bifurcation.

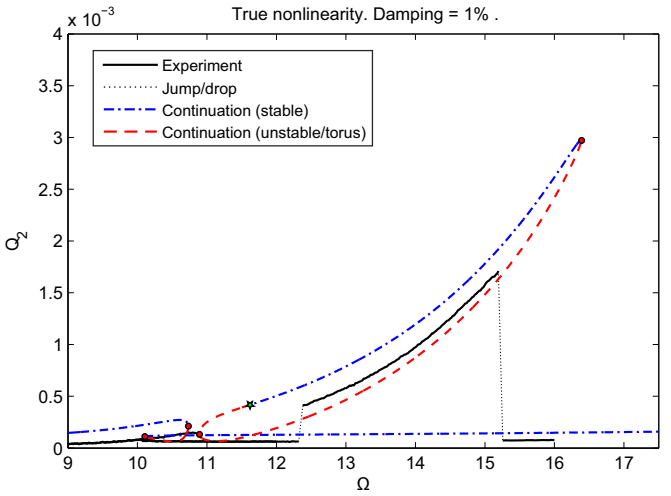

Fig. 14. Comparison of experimental results to continuation model using Eq. (1). Q_2 represents the amplitude of the second modal variable at the third harmonic of the drive frequency, with the modeshape scaled to give unit tip displacement. Forcing amplitude is 2.0 N. Circular markers on continuation results indicate fold bifurcations, star indicates a torus bifurcation.

upper jump frequencies, it may be noted from Fig. 10 that the drive frequency (and most significant) response reaches a phase of approximately 90° at the upper drop down in all cases shown, suggesting that the true peak has been reached and supporting the theory that the error lies within the damping model. The lower isola drop down frequencies occur when the response is approaching the region of quasi-periodic response described in Section 4.3. The vibration control strategy is based upon the assumption of periodic response, and therefore is likely to experience considerable difficulty as it approaches this region, potentially causing it force the beam outside the basin of attraction for this model. Therefore a refined experimental approach is required to thoroughly examine the response in these regions.

Fig. 14 shows the comparison between experiment and continuation in terms of the second modal variable Q_2. In this case the match is qualitatively less good than for Q_1, Fig. 13, although the qualitative shape of the isola region is captured reasonably well. The poorer agreement can be explained by noting that the scale of these results is much smaller than those given in Fig. 13. This means that errors within measurement, and those due to the assumption of a two-mode proportionally damped system, become significant. It is thought that the use of more sophisticated modelling could improve accuracy for these results in future work.

The bifurcations shown by the continuation analysis shed considerable light on the experimental response. The fold bifurcations at approximately 10.0 Hz, 10.7 Hz and 16.0 Hz correspond to the $S^{-}_{1,2}$ jump up, $S^{-}_{1,2}$ jump down and $S^{+}_{1,2}$ upper jump down frequencies respectively. However, the continuation also shows a torus bifurcation at approximately 11.6 Hz, leading to a region of quasiperiodicity between there and the lower fold bifurcation on the isola loop, as encountered during the test. This analysis also shows why the complex region of peak displacement shown in Fig. 6 cannot be fully revealed in experiment; the bifurcation structure shows that the majority of branches in this region are unstable, hence only one part of this complex loop of backbones can be followed.

Despite the sensitivity of the continuation model to parameters such as damping, it consistently showed a qualitatively similar structure of bifurcations, with no torus bifurcation occurring on the primary branch. Therefore, it can be confirmed that the isola is not connected to the primary branch via a quasiperiodic region, and that the experimental isola is genuine.

6. Conclusions and future work

This work has shown experimentally how a local nonlinearity can introduce rich dynamics into a structure that would otherwise form a classical example of linear modal dynamics. In particular, the presence of a 3:1 internal resonance has been shown to cause effects including isolated response regions and quasiperiodicity. Many of the practical issues in exploring these features experimentally have been discussed.

The response to harmonic forcing has been shown to be largely governed by a complex backbone structure, derived using the method of normal forms with the modal properties of the underlying linear structure. At many frequencies, the backbone structure is seen to have a far more significant effect than the forcing amplitude. Finally, continuation analysis of the forced and damped system has revealed a pattern of bifurcations that qualitatively explain many of the observed responses, and show reasonable quantitative agreement, albeit potentially limited numerically by the use of a simplistic damping model, and possible experimental control issues near the torus bifurcation.

The presence of these rich dynamical phenomena pose a formidable challenge in identifying an underlying dynamic model

from purely experimental data, in a manner similar to that achieved by the practice of experimental modal analysis for linear structures. It is hoped that this work can provide an invaluable test case for future research efforts to achieve this goal.

Acknowledgements

The research leading to these results has received funding from EPSRC grant number EP/G036772/1. A.D. Shaw and M.I. Friswell received funding from the European Research Council under the European Union's Seventh Framework Programme (FP/2007-2013)/ERC Grant Agreement no. [247045]. In addition, Simon Neild and Tom Hill are supported by an EPSRC Fellowship (EP/K005375/1).

The data presented in this work is openly available from the University of Bristol repository at http://dx.doi.org/10.5523/bris.1ovr9cp1whfbw1tfpql4hf10sq or from http://dx.doi.org/10.5281/zenodo.48133.

References

[1] D.J. Wagg, S.A. Neild, Nonlinear Vibration with Control, Springer, Dordrecht, 2009.
[2] M. Amabili, Nonlinear Vibrations and Stability of Shells and Plates, Cambridge University Press, New York, 2008.
[3] R.W. Ogden, Non-Linear Elastic Deformations, Dover Publications, New York, 1997.
[4] G.M. Rebeiz, RF MEMS: Theory, Design, and Technology, John Wiley & Sons, Hoboken, 2004.
[5] A. Carrella, Passive Vibration Isolators with High-Static-Low-Dynamic-Stiffness, VDM Verlag Dr. Muller, Saarbrücken, 2010.
[6] M.F. Daqaq, R. Masana, A. Erturk, D.D. Quinn, On the role of nonlinearities in vibratory energy harvesting: a critical review and discussion, Appl. Mech. Rev. 66 (4) (2014) 040801.
[7] D. Ewins, Modal testing: theory, practice, and application, in: Mechanical Engineering Research Studies: Engineering Dynamics Series, Research Studies Press, Baldock, 2000.
[8] K. Worden, G.R. Tomlinson, Nonlinearity in Structural Dynamics, Institute of Physics, Bristol, 2001.
[9] G. Kerschen, K. Worden, A.F. Vakakis, J.-C. Golinval, Past, present and future of nonlinear system identification in structural dynamics, Mech. Syst. Signal Process. 20 (3) (2006) 505–592.
[10] S.W. Shaw, C. Pierre, Normal modes for non-linear vibratory systems, J. Sound Vib. 164 (1) (1993) 85–124.
[11] G. Kerschen, M. Peeters, J. Golinval, A. Vakakis, Nonlinear normal modes, part i: a useful framework for the structural dynamicist, Mech. Syst. Signal Process. 23 (1) (2009) 170–194. Special Issue: Non-linear Structural Dynamics.
[12] A.H. Nayfeh, Nonlinear Interactions, Wiley, New York, 2000.
[13] G. Rega, R. Alaggio, F. Benedettini, Experimental investigation of the nonlinear response of a hanging cable. part i: local analysis, Nonlinear Dyn. 14 (2) (1997) 89–117.
[14] M. Amabili, Nonlinear vibrations of rectangular plates with different boundary conditions: theory and experiments, Comput. Struct. 82 (3132) (2004) 2587–2605. Nonlinear Dynamics of Continuous Systems.
[15] C.L. Zaretzky, M.R.M. Crespo da Silva, Experimental investigation of non-linear modal coupling in the response of cantilever beams, J. Sound Vib. 174 (2) (1994) 145–167.
[16] F. Benedettini, G. Rega, Experimental investigation of the nonlinear response of a hanging cable. part ii: global analysis, Nonlinear Dyn. 14 (2) (1997) 119–138.
[17] H.J.R. Westra, M. Poot, H.S.J. van der Zant, W.J. Venstra, Nonlinear modal interactions in clamped–clamped mechanical resonators, Phys. Rev. Lett. 105 (September) (2010) 117205.
[18] M.F. Platten, J.R. Wright, J.E. Cooper, G. Dimitriadis, Identification of a nonlinear wing structure using an extended modal model, J. Aircr. 46 (5) (2009) 1614–1626.
[19] J.M. Londoño, J. E. Cooper, S.A. Neild, Vibration testing of large scale nonlinear structures, in: Proceedings of ISMA 2014, 2014.
[20] J.M. Londono, J.E. Cooper, Experimental identification of a system containing geometric nonlinearities, in: J. De Clerck (Ed.), Topics in Modal Analysis I, vol. 7, Conference Proceedings of the Society for Experimental Mechanics Series, Springer International Publishing, 2014, pp. 253–260.
[21] J.P. Noël, L. Renson, G. Kerschen, Complex dynamics of a nonlinear aerospace structure: experimental identification and modal interactions, J. Sound Vib. 333 (12) (2014) 2588–2607.
[22] H. Cho, B. Jeong, M.-F. Yu, A.F. Vakakis, D.M. McFarland, L.A. Bergman, Nonlinear hardening and softening resonances in micromechanical cantilever-nanotube systems originated from nanoscale geometric nonlinearities, Int. J. Solids Struct. 49 (1516) (2012) 2059–2065.
[23] F. Thouverez, Presentation of the ecl benchmark, Mech. Syst. Signal Process. 17 (1) (2003) 195–202.
[24] G.V. Demarie, R. Ceravolo, D. Sabia, P. Argoul, Experimental identification of beams with localized nonlinearities, J. Vib. Control 17 (11) (2011) 1721–1732.
[25] M. Peeters, G. Kerschen, J. Golinval, Modal testing of nonlinear vibrating structures based on nonlinear normal modes: experimental demonstration, Mech. Syst. Signal Process. 25 (4) (2011) 1227–1247.
[26] R.J. Kuether, L. Renson, T. Detroux, C. Grappasonni, G. Kerschen, M.S. Allen, Nonlinear normal modes, modal interactions and isolated resonance curves, J. Sound Vib. 351 (2015) 299–310.
[27] T. Detroux, J.P. Noël, L. Masset, G. Kerschen, L.N. Virgin, Numerical study of the intrinsic features of isolas in 2-dof nonlinear system, in: Proceedings of ICEDyn, 2015.
[28] S.A. Neild, D.J. Wagg, Applying the method of normal forms to second-order nonlinear vibration problems, Proc. R. Soc. A 467 (2128) (2010) 1141–1163.
[29] A.F. Vakakis, O.V. Gendelman, L.A. Bergman, D.M. McFarland, G. Kerschen, Y.S. Lee, Nonlinear Targeted Energy Transfer in Mechanical and Structural Systems, vol. 156, Springer Science & Business Media, Dordrecht, 2008.
[30] A.H. Nayfeh, D.T. Mook, Nonlinear Oscillations, John Wiley & Sons, New York, 2008.
[31] Labview System Design Software.
[32] D.A.W. Barton, B.P. Mann, S.G. Burrow, Control-based continuation for investigating nonlinear experiments, J. Vib. Control 18 (4) (2012) 509–520.
[33] A. Cammarano, T.L. Hill, S.A. Neild, D.J. Wagg, Bifurcations of backbone curves for systems of coupled nonlinear two mass oscillator, Nonlinear Dyn. 77 (1–2) (2014) 311–320.
[34] T.L. Hill, A. Cammarano, S.A. Neild, D.J. Wagg, Interpreting the forced responses of a two-degree-of-freedom nonlinear oscillator using backbone curves, J. Sound Vib. 349 (2015) 276–288.
[35] S.A. Neild, A.R. Champneys, D.J. Wagg, T.L. Hill, A. Cammarano, The use of normal forms for analysing nonlinear mechanical vibration, Philos. Trans. R. Soc. A 373 (2051) (2015) 20140404.
[36] E.J. Doedel, with major contributions from A.R. Champneys, T.F. Fairgrieve, Yu.A. Kuznetsov, F. Dercole, B.E. Oldeman, R.C. Paffenroth, B. Sandstede, X.J. Wang, C. Zhang, AUTO-07P: Continuation and Bifurcation Software for Ordinary Differential Equation, Concordia University, Montreal, Canada, 2008, Available at: ⟨http://cmvl.cs.concordia.ca⟩.